International Journal of Environment, Agriculture and Biotechnology
Vol-11, Issue-5; Sep-Oct, 2026
Peer-Reviewed International Journal
Journal Home Page Available: https://ijeab.com/
Journal DOI: 10.22161/ijeab

Parcel-Level Land Cover and Soil Fertility Mapping using Multi-Sensor Satellite Imagery, Cadastral Overlays and Soil Health Card Records in a Semi-Arid Taluka of Saurashtra, Gujarat, India

Hardeep Kumar*[1], N. K. Gontia[2], Pritam Das[2] and P. A. Pandya[2]

[1]Gujarat State Watershed Management Agency (GSWMA), Gandhinagar, Gujarat, India
[2]Junagadh Agricultural Univrsity, Junagadh, Gujarat, India
*Corresponding Author Email:- hardeep47@gmail.com

Received: 23 Sep 2026; Received in revised form: 19 Oct 2026; Accepted: 25 Oct 2026; Available online: 31 Oct 2026
©2026 The Author(s). Published by Infogain Publication. This is an open-access article *under* the CC BY license (https://creativecommons.org/licenses/by/4.0/)

Abstract— *Reliable, spatially explicit information on land cover and soil fertility is a prerequisite for micro-level planning of land and water resources in rainfed, groundwater-dependent agricultural regions. This study demonstrates a workflow that links multi-sensor Indian Remote Sensing satellite data, digitised cadastral records and Soil Health Card (SHC) data for Amreli Taluka (83,112 ha), Saurashtra, Gujarat. CARTOSAT-1 panchromatic, IRS-P6 LISS-III and LISS-IV scenes were georeferenced and overlaid with village boundaries and survey-number polygons for seven randomly selected villages. A LISS-III scene of 31 January 2009 was classified with a maximum-likelihood supervised classifier using training signatures derived from a false colour composite, and the result was evaluated with a confusion matrix and the kappa coefficient. Nutrient status (N, P, K, organic carbon) and soil reaction (pH, electrical conductivity) from the SHCs were joined to cadastral polygons and mapped at survey-number level for Sanosara village. Dense, medium and poor agriculture occupied 28.27%, 22.24% and 14.23% of the taluka, respectively, which together with fallow land (16.81%) accounted for 81.55% of the area; habitation covered 12.01%, waste or eroded land 4.73% and water bodies 1.71%. The summary statistics reported with the matrix are an average accuracy of 83.08%, an overall accuracy of 79.32% and a kappa coefficient of 0.754 (standard deviation 0.00165; 95% confidence limit ±0.00324). SHC records showed predominantly medium nitrogen, low phosphorus and high potash, with normal pH (6.5-8.2) and electrical conductivity below 1 dS m^{-1}. The cadastral-level approach converts farm-scale soil data into mappable, plot-specific recommendations, but accuracy reporting, class design and sampling density need strengthening before the maps are used operationally. The workflow is transferable to other talukas where SHC and cadastral data exist.*

Keywords— ***IRS-P6 LISS-III, Maximum likelihood classification, Micro-level planning, Soil fertility mapping***

HIGHLIGHTS

- Cadastral overlays on multi-sensor satellite imagery enable plot-level visibility.
- Cultivated land covers 64.73%, but dense-medium agriculture confusion limits accuracy.
- Soil Health Cards show low phosphorus, medium nitrogen, high potash.

I. INTRODUCTION

Land and water are the two resources on which dryland agriculture in western India depends, and both are under increasing pressure from population growth, variable

monsoon rainfall and declining groundwater tables. Planning for their sustainable use has traditionally been done at the macro level, with district or state aggregates guiding investment. Such aggregates conceal the spatial heterogeneity that determines whether a particular field, village or cluster of villages can sustain a given cropping system. Decentralised, village-level or "micro-level" planning therefore needs information at a resolution fine enough to resolve individual land parcels and to link them to the farmers who manage them. India has a long record of remote-sensing-based resource inventories (Kasturirangan, 1995; Puri, 2007), and local-level planning has been supported by natural-resource databases and decision support systems (Acharya et al., 2011; Gupta et al., 2001; Bariar et al., 2004), by watershed-based resource management (Krishna, 1996) and, through watershed development projects, by programmes whose performance has been formally evaluated (Kerr et al., 2002).

Satellite remote sensing has long been the main source of synoptic land cover information, and the methods used to turn imagery into thematic maps have evolved from visual interpretation and per-pixel supervised and unsupervised classifiers (Lillesand et al., 2015) to ensemble learners and deep neural networks. Reviews of land use and land cover (LULC) classification emphasise that, despite decades of progress, issues of multi-source, multi-temporal and multi-level analysis, robustness, quality and scalability remain open (Macarringue et al., 2022). Deep-learning approaches now dominate the recent literature and offer clear gains in accuracy where large labelled datasets exist, yet they depend on training samples that are scarce for many agricultural regions, and classic algorithms such as maximum likelihood, support vector machines and decision trees remain widely used (Zhao et al., 2023; Digra et al., 2022). For operational work in data-poor districts, where field-verified samples are limited and analysts need transparent, reproducible procedures, the supervised statistical classifier retains practical value, provided its accuracy is reported honestly.

A second strand of work concerns the mapping of soil properties. Digital soil mapping has matured around the idea of using remote sensing and other environmental covariates either as a substitute for analytical measurements or as predictors of soil-forming factors (Richer-de-Forges et al., 2023). A global review of broad-scale digital soil mapping found that most studies targeted soil organic matter or carbon, that texture fractions were comparatively well predicted, and that soil depth and coarse fragments were poorly predicted; the authors called for rescued legacy data, better sampling designs and representative covariates (Chen et al., 2022). These findings are relevant to India, where an unusually dense source of measured soil data already exists in the form of Soil Health Cards. The Soil Health Card scheme, launched nationally in 2015 after earlier state-level initiatives, provides plot-wise nutrient status and fertiliser recommendations; a recent systematic review reports that the scheme has been associated with yield increases of 5-6% and reductions in chemical fertiliser use of 8-10%, while also identifying institutional gaps that limit its impact (Timilsina et al., 2025). The idea of a soil health card as a decision-support tool for balanced fertilisation predates the national scheme (Thiyageshwari et al., 2006). Because each card is tied to a survey number, the data are intrinsically cadastral and can be mapped directly if the cadastral polygons are digitised and georeferenced. Where point observations must instead be converted into continuous surfaces, geostatistical interpolation such as kriging has long been used (Largueche, 2006), but it needs a sample that is dense and representative enough to support the interpolation.

The bridge between parcel-scale records and satellite imagery is the agricultural parcel itself. A comprehensive review of agricultural parcel and boundary delineation notes that the number of studies using very high resolution imagery has grown exponentially since 2019, that satellite imagery supplies the large majority of data sources, and that smallholder systems with small, irregular and fragmented fields remain the hardest setting for automated delineation (Zheng et al., 2026). Cadastral boundaries, where they exist, offer a stable alternative to automatically derived boundaries, but they must be registered precisely to imagery for the combination to be useful. Systematic reviews of crop mapping and crop monitoring similarly stress the value of combining multiple sensors and ancillary information for agricultural applications (Alami Machichi et al., 2023; Joshi et al., 2023; Wu et al., 2023). Remote sensing has also been applied to irrigated agriculture for several decades, with examples ranging from research to practical use (Bastiaanssen et al., 2000).

Against this background, the present study documents and critically evaluates a workflow applied to Amreli Taluka in the Saurashtra region of Gujarat. The objectives were (i) to georeference and overlay CARTOSAT-1, IRS-P6 LISS-III and LISS-IV imagery with cadastral and village boundaries so that individual survey numbers can be located on the images; (ii) to derive a land use/land cover map for the taluka from a LISS-III scene using a supervised maximum-likelihood classifier and to quantify its accuracy; and (iii) to map nutrient status and soil reaction from Soil Health Card records at survey-number level and to summarise the status of seven selected villages. The intention is not only to report the maps but also to examine how reliable they are and what is needed to make such products dependable inputs to village-level planning.

II. MATERIALS AND METHODS

Study area

Amreli Taluka lies in Amreli District in the Saurashtra peninsula of Gujarat, between 21°24′ and 21°43′ N latitude and 70°59′ and 71°24′ E longitude (Fig. 1), with a geographical areas of 83,112 ha. About 80% of the population depends on agriculture as its main occupation and groundwater is the principal irrigation source. The area is predominantly dry-land farmed, with groundnut and sesame as the main kharif crops, wheat and coriander in the rabi season, summer sesame in irrigated pockets, and vegetables and orchards (coconut, mango and sapota) on the remaining cropland. The taluka is crossed by a network of roads and a railway line and contains numerous settlements; Fig. 2 shows the transport network, settlement points and village boundaries on which the cadastral work was based.

Seven villages were selected at random for detailed parcel-level work, *i.e.*, Bhandariya Mota, Sanosara, Vadhera, Rangapur, Navakhijadiya, Bhandariya Nana and Mangvapal (Fig. 3). Sanosara was used as the demonstration village for survey-number-level overlays and nutrient maps.

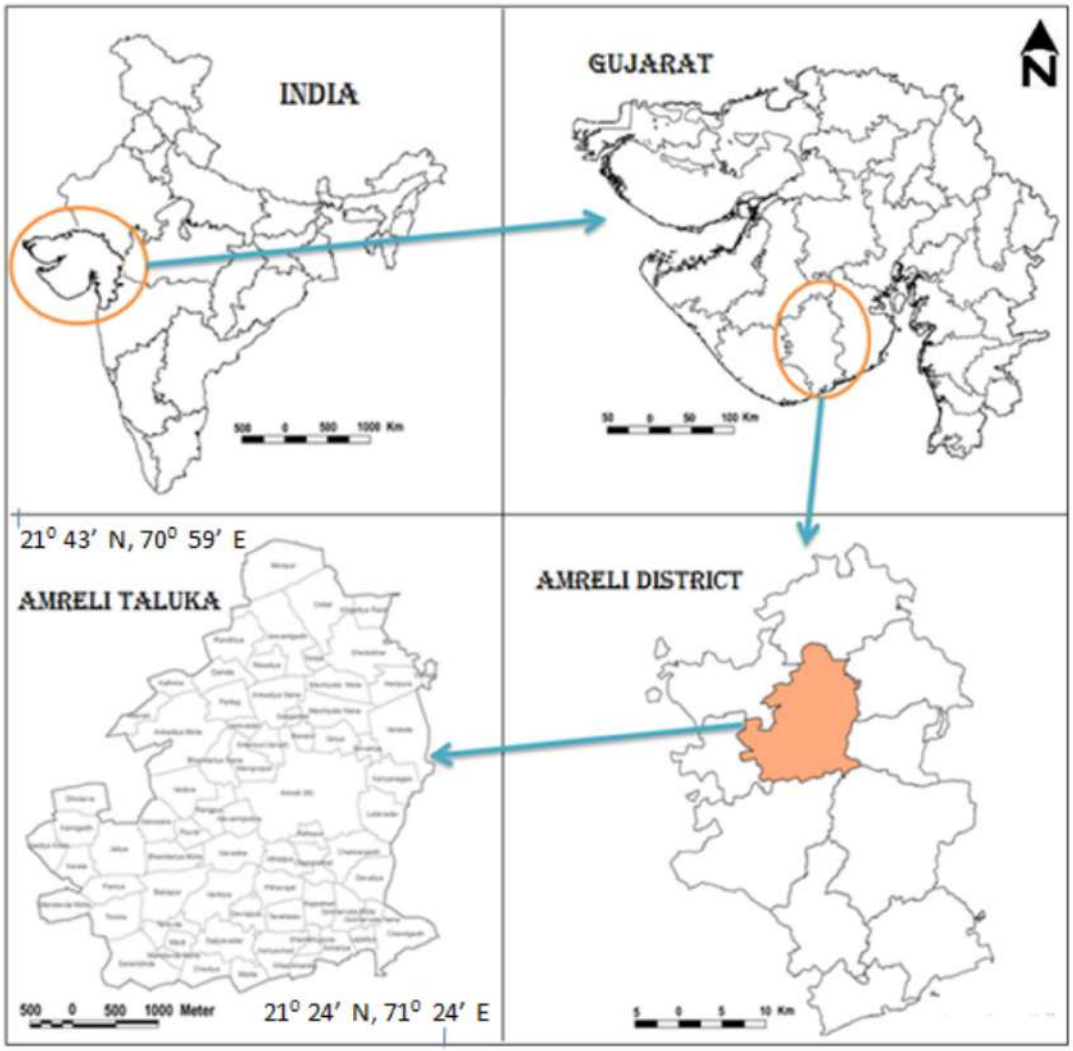


Fig. 1. Location of Amreli Taluka within India, Gujarat state and Amreli District.

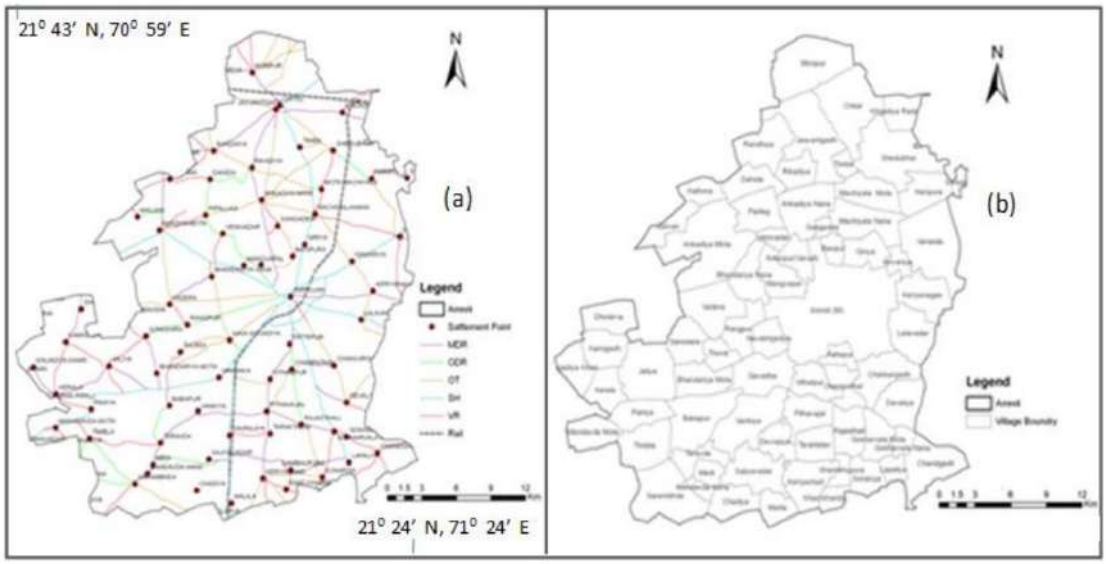


Fig. 2. (a) Roads, railway and settlement points and (b) village boundaries of Amreli Taluka.

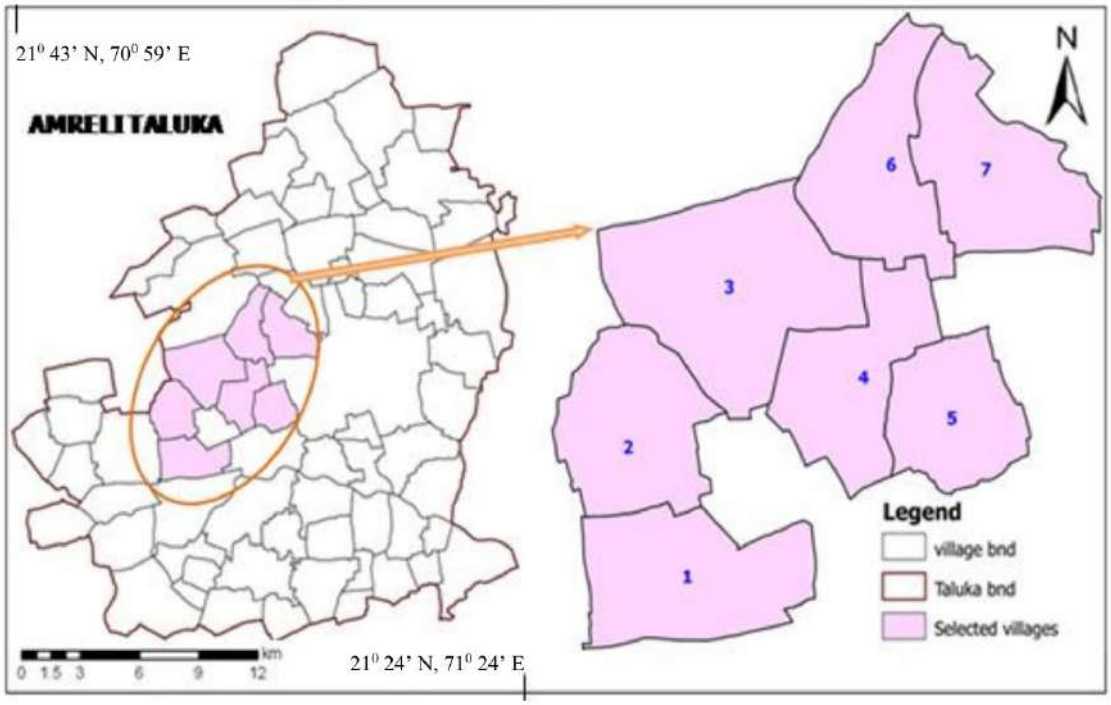


Fig. 3. Layout of the seven selected villages within Amreli Taluka (1. Bhandariya Mota, 2. Sanosara, 3. Vadhera, 4. Rangapur, 5. Navakhijadiya, 6. Bhandariya Nana, 7. Mangvapal).

Satellite and ancillary data

Three Indian Remote Sensing data types were used (Table 1). CARTOSAT-1 panchromatic data (nominal spatial resolution of 2.5 m) supplied the finest geometric detail for locating plot boundaries. IRS-P6 (Resourcesat-1) LISS-IV scenes (nominal 5.8 m multispectral) provided intermediate resolution, and IRS-P6 LISS-III (nominal 23.5 m, four spectral bands) was used for taluka-wide classification. All scenes were procured from the Bhaskaracharya Institute for Space Applications and Geo-informatics (BISAG), Gandhinagar. Google Earth Pro images were consulted as a visual reference. A district map of Amreli provided district, taluka and village boundaries, and scanned cadastral sheets gave village boundaries and survey numbers for the selected villages.

Table 1: Satellite data used in the study.

Sr. no.	Satellite	Sensor	Path/Row	Date of pass
1	CARTOSAT-1	PAN	502/297	17 Feb 2006
2	CARTOSAT-1	PAN	502/298	17 Feb 2006
3	IRS-P6	LISS-III	92/57	31 Jan 2009
4	IRS-P6	LISS-IV	201/102	12 May 2008
5	IRS-P6	LISS-IV	202/80	24 Feb 2009
6	IRS-P6	LISS-IV	202/96	31 Jan 2009
7	IRS-P6	LISS-IV	203/57	30 Mar 2009

Soil Health Card data for the seven villages were downloaded from the Government of Gujarat web site. Each card records the soil type, the fertility status of the plot (nitrogen, phosphorus, potash and organic carbon, in qualitative classes), pH and electrical conductivity, and the name of the farmer who holds the survey number. The scheme was started in 2008-09 on a per-plot basis, so the cards provide a soil record for individual fields.

Georeferencing and cadastral digitisation

Scanned maps were registered to the satellite images and converted to vector data by on-screen digitisation. In ArcGIS 9.2, each scanned sheet was added as a raster, a polygon shapefile was created, and village and survey-number boundaries were traced with the editing tools using edge-snapping to reduce digitising error. Image geometry was handled in PCI Geomatica 10.1, where an affine transformation model was applied to the cadastral sheets and image scenes were clipped to the study area through a vector mask and subset dialogue. After registration, the cadastral vectors were superimposed on each image and checked visually so that every survey-number boundary coincided with a field boundary or road visible on the imagery. Overlays were produced for all three sensors to allow a like-for-like comparison of how well each sensor resolves plot geometry. Integrating spatial databases of this kind with quantitative models is a long-standing theme in land resource assessment (Stehman, 1997).

Image classification

Land cover was derived from the LISS-III scene of 31 January 2009, which falls at the end of the May-January cotton growing season analysed in the companion study. A false colour composite (FCC) was displayed and used to select training polygons for seven information classes: water bodies, dense agriculture, medium agriculture, poor agriculture, fallow land, habitation or establishment, and waste or eroded land. The signature of each class, comprising mean, standard deviation, variance and the covariance matrix of the selected pixels in the five channels held in the signature file, was inspected for separability. Dense agriculture and fallow land were each split into two spectral sub-classes during training so that internal spectral variability was represented. The image was then classified using the maximum-likelihood decision rule, in which each pixel is assigned to the class for which its probability of membership, assuming a multivariate normal distribution, is highest (Lillesand et al., 2015). The methods chapter of the source thesis also describes K-means clustering as a classification option, but the results and abstract report the supervised maximum-likelihood map, which was therefore adopted here. Class areas were extracted from the attribute table of the classified raster using the pixel size of the scene.

Accuracy assessment

Classification accuracy was evaluated with an error (confusion) matrix in which rows represent reference classes and columns the mapped classes, with the percentage of pixels of each reference class falling into each mapped class reported. The diagonal elements give per-class accuracy. Overall measures and the kappa coefficient of agreement with its confidence limits were computed from the matrix. Because the thesis from which the data derive reports different values for “average” and “overall” accuracy, both are reported below and an independent pixel-weighted recalculation from the tabulated row percentages was added as a consistency check. Standard treatments of thematic accuracy recommend reporting the full confusion matrix and per-class accuracy alongside any summary index (Stehman, 1997), and this principle was followed here.

Mapping soil fertility and reaction from Soil Health Cards

For each village, the SHC records were keyed to survey numbers and joined to the digitised survey-number polygons through a common identifier. Nutrient classes

were retained as reported (nitrogen, phosphorus and potash as low, medium or high; organic carbon as low, medium or optimum; pH as normal within 6.5-8.2; electrical conductivity as normal below 1 dS m^{-1}). Polygons with an SHC record were coloured by class and displayed on the CARTOSAT-1 image together with all survey-number boundaries, so that polygons without a card remain visible as unmapped. This produced one map per attribute for Sanosara village. A village-level summary was prepared by recording the dominant class of each nutrient in the seven villages. No spatial interpolation was applied, so unsampled plots remain unmapped instead of being assigned values by methods such as kriging (Largueche, 2006). The overall methodology is presented in Fig. 4.

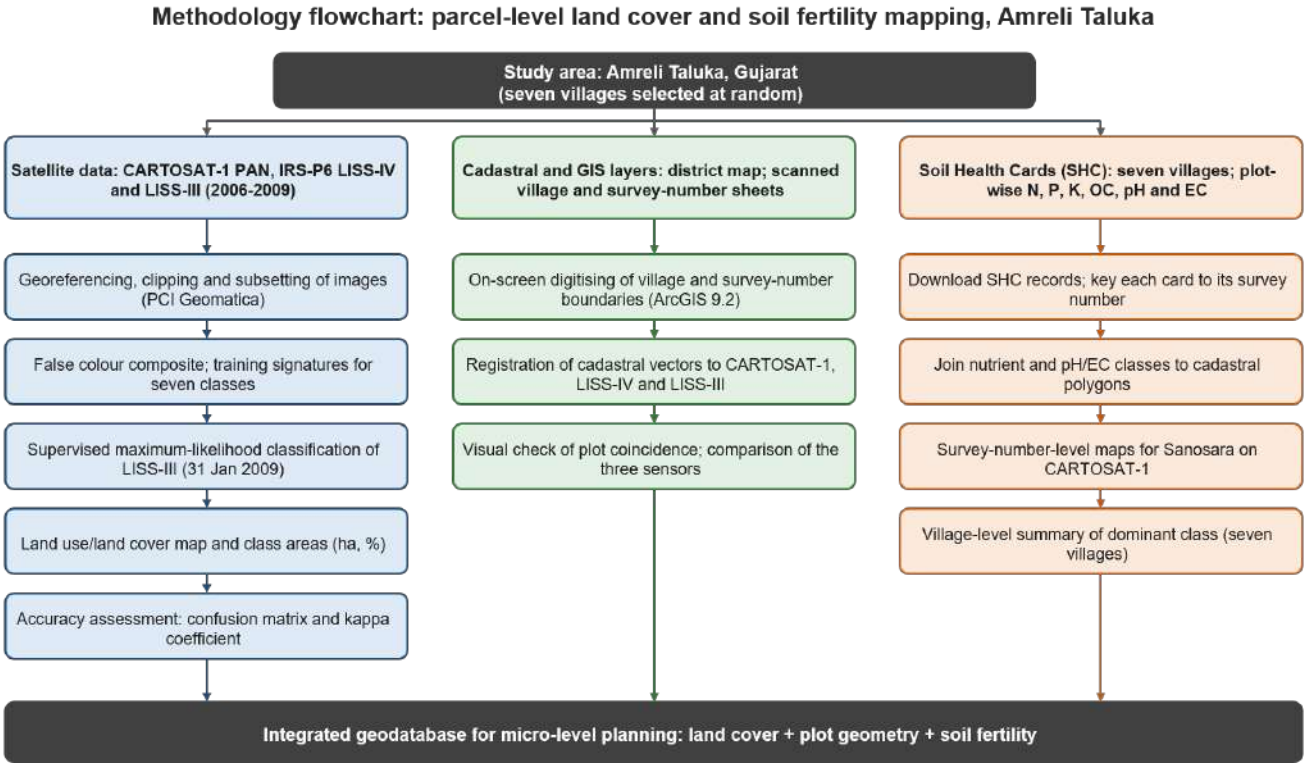


Fig. 4. The overall methodology adopted in this study

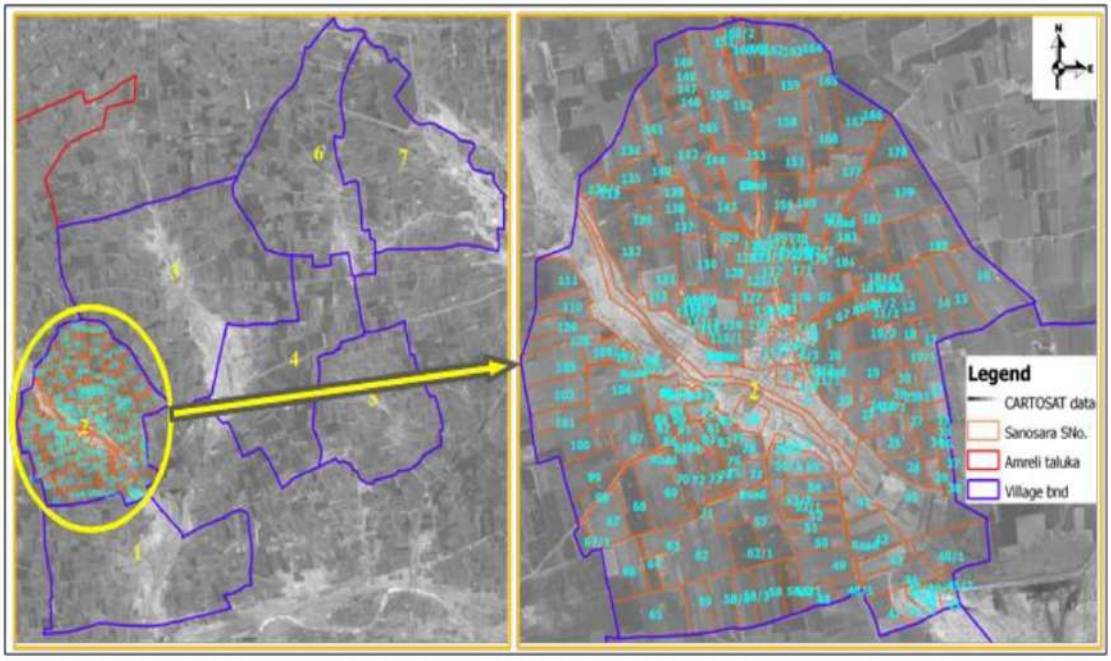


Fig. 5. Cadastral map of Sanosara village with survey numbers superimposed on CARTOSAT-1 data

III. RESULTS AND DISCUSSION

Multi-sensor overlays and plot-level visibility

Overlaying the village boundaries and survey-number polygons on the three sensors showed clear differences in how well plots could be recognised. On CARTOSAT-1 (Fig. 5) the individual field patterns, tracks, the drainage line crossing Sanosara and the village built-up core were easily identified, and each survey-number polygon could be matched to a visible field unit. On LISS-III (Fig. 6) the cadastral grid was much finer than the pixel size, so that a single pixel frequently spanned two or more survey numbers. On LISS-IV (Fig. 7) larger plots were distinguishable, though small plots and narrow strips were mixed.

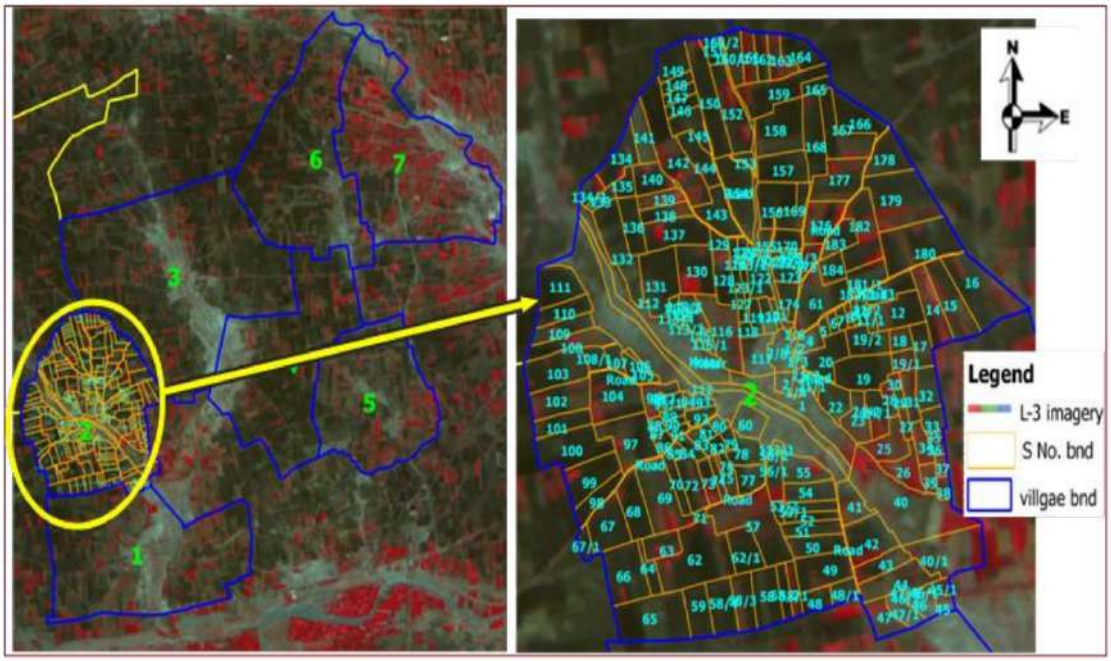


Fig. 6. Cadastral map of Sanosara village with survey numbers superimposed on the LISS-III image

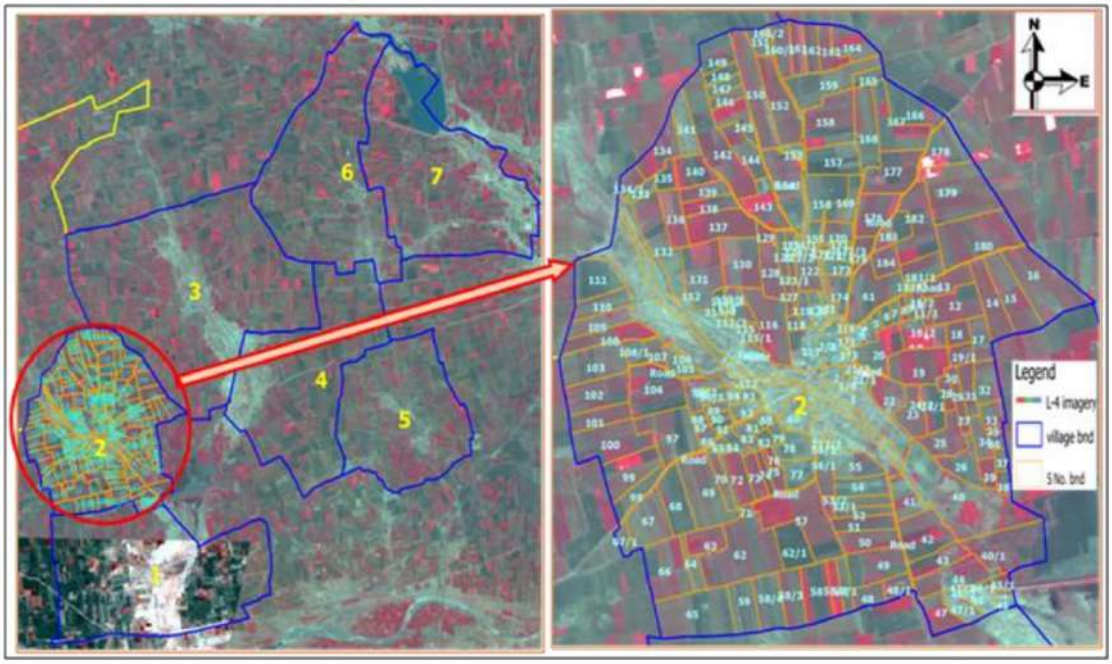


Fig. 7. Cadastral map of Sanosara village with survey numbers superimposed on the LISS-IV image

This ordering is consistent with the nominal resolutions of the sensors and with the general finding of the parcel-delineation literature that spatial resolution is the primary determinant of recoverable geometric information in fragmented smallholder landscapes (Zheng et al., 2026). The practical consequence is a division of labour: LISS-III is adequate for a taluka-wide land cover inventory in which the mapping unit is a class patch, whereas plot-level work needs CARTOSAT-1 or LISS-IV, at least as a visual backdrop. A fused product, in which the multispectral information of LISS-IV or LISS-III is sharpened with the panchromatic CARTOSAT-1 band, would be the logical next step and corresponds to the multi-source data integration that reviews identify as a continuing challenge (Macarringue et al., 2022; Zheng et al., 2026). The present study did not carry out fusion, and the three overlays were interpreted separately.

A caveat applies to all overlays. The CARTOSAT-1 scene dates from February 2006 and the cadastral maps from earlier surveys, whereas the SHC records were collected after 2008. Field amalgamation, subdivision and changes in tracks over a three-year gap can introduce small mismatches between polygons and what is visible on the image. Visual coincidence was verified, but no positional error statistic, such as root-mean-square error against ground control points, is available.

Training signatures and class separability

The signature statistics of the training classes are shown in Fig. 8. The mean digital numbers in the five channels differ markedly between classes. Water bodies and habitation have distinct channel means, and the sub-classes of dense agriculture, fallow land and medium agriculture differ especially in the near-infrared channel, the channel that captures the strong reflectance of healthy vegetation. Standard deviations are small relative to the differences between class means for most classes, which indicates compact training clusters. The two dense-agriculture signatures, trained on 2,935 and 594 sample pixels respectively in the displayed statistics, illustrate how a single information class can contain more than one spectral population; this decision to split the class is revisited when accuracy is discussed.

Land use and land cover of Amreli Taluka

The false colour composite and the supervised classification are shown side by side in Fig. 9. In the FCC, dense healthy vegetation appears in red tones, fallow and bare surfaces in light cyan and white, and water as dark blue to black. The classified map reproduces this pattern, with the drainage network, the larger settlements and the fallow land of the southern part of the taluka clearly delineated.



Fig.8. Training signature statistics (mean and standard deviation by channel) for the land cover classes derived from the LISS-III image

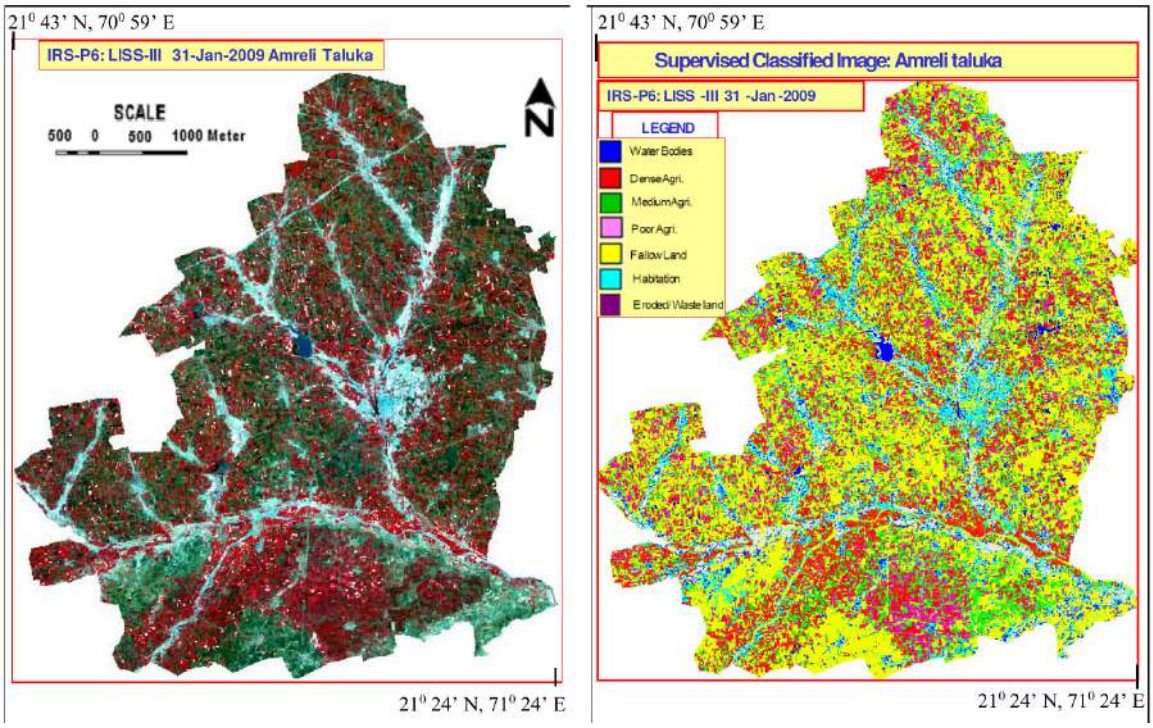


Fig. 9. IRS-P6 LISS-III false colour composite of 31 January 2009 (left) and the supervised land use/land cover classification (right) of Amreli Taluka

Table 2: Land use/land cover classes of Amreli Taluka derived from the LISS-III image of 31 January 2009

Class	Area (ha)	Share of taluka (%)	Share of mapped agricultural and fallow land (%)
Water bodies	1,425	1.71	-
Dense agriculture	23,493	28.27	34.7
Medium agriculture	18,484	22.24	27.3
Poor agriculture	11,825	14.23	17.4
Fallow land	13,974	16.81	20.6
Habitation/establishment	9,980	12.01	-
Waste/eroded land	3,931	4.73	-
Total	83,112	100.00	100.0

Cultivated land, defined as dense, medium and poor agriculture, covered 53,802 ha (64.73% of the taluka), and with fallow land the agricultural land base reached 67,776 ha (81.55%). Habitation, mainly the many small villages and the town of Amreli, occupied 12.01% of the taluka, a share that is high for a rural taluka and that reflects the dense network of settlements visible in Fig. 2. Land-cover maps of this kind can be repeated at later dates to follow land development over time, as has been done for urban expansion elsewhere (Markon, 2003). Waste and eroded land were limited to 4.73%, and water bodies, mostly ponds and submerged areas, to 1.71%.

The sub-division of cultivated land by vegetation density deserves a careful reading. Of the cultivated area, dense agriculture accounts for 43.7%, medium for 34.4% and poor for 22.0%. These shares differ from the 60%, 30% and 10% quoted in the original thesis narrative, which cannot be

reproduced from the tabulated areas; the table values are used here. Because the image was acquired on 31 January, the "dense" class represents fields with high canopy vigour at that date, which may include cotton and other irrigated crops. Vigour classes on a single date should not be read as crop-type areas, and any statement about the area under a particular crop would require time-series data and field verification.

The 16.81% of fallow land recorded in January needs similar caution. Part of it may be fields harvested early, fields awaiting rabi sowing under residual moisture, or land left idle for lack of irrigation. Because rainfed fields in Saurashtra are often sown only once in the monsoon, high January fallow in a dry-land taluka is plausible, but a second date in the rabi or summer season would be needed to distinguish permanent fallow from seasonal fallow.

Classification accuracy

Table 3 condenses the confusion matrix into per-class accuracy. Most classes were correctly classified in 83-91% of reference pixels. Water bodies (87.72%), habitation (85.49%), waste or eroded land (85.94%), medium agriculture (85.76%), poor agriculture (83.36%), fallow land (88.53% and 90.79% for the two sub-classes) and the first dense-agriculture sub-class (88.01%) all met or approached the accuracy thresholds commonly accepted for thematic maps. The principal exception is the second dense-agriculture sub-class, which was correctly assigned in only 35.19% of its 17,202 reference pixels, with 52.49% allocated to medium agriculture. This sub-class holds by far the largest number of pixels of any agricultural class in the matrix, so its confusion has a disproportionate effect on both overall accuracy and the area estimates of the dense and medium agriculture classes.

Table 3: Per-class accuracy from the confusion matrix of the LISS-III classification

Reference class	Pixels	Correctly classified (%)	Main confusion (%)
Dense agriculture-1	2,935	88.01	Unclassified 10.97
Dense agriculture-2	17,202	35.19	Medium agriculture 52.49
Medium agriculture	597	85.76	Poor agriculture 7.71
Poor agriculture	613	83.36	Medium agriculture 9.14
Fallow land-1	13,814	88.53	Unclassified 9.12
Fallow land-2	3,920	90.79	Fallow land-1 3.24
Water body	1,735	87.72	Unclassified 12.28
Habitation	2,823	85.49	Waste/eroded 6.67
Waste/eroded land	8,993	85.94	Habitation 4.47

The summary statistics reported with the matrix are an average accuracy of 83.08%, an overall accuracy of 79.32% and a kappa coefficient of 0.754 (standard deviation 0.00165; 95% confidence limit ±0.00324). The original narrative treats the 83.08% value as the overall accuracy, while the table lists it as the average. As a consistency check, the nine diagonal percentages in Table 3 average 81.2%, and weighting them by the number of reference pixels in each class gives an overall accuracy of about 70.5%. The difference from the reported 79.32% suggests that the reported indices were computed on a different, possibly cleaned, sample or after merging sub-classes. The effect of merging is relevant because combining spectrally confusable classes inflates apparent accuracy, a point emphasised in discussions of thematic map assessment. The only defensible reading is that overall accuracy lies between roughly 70% and 80%, depending on the sample and on whether sub-classes are merged, and that the kappa value of 0.754, which would normally be called substantial agreement, may overstate performance for the two dense-agriculture sub-classes.

Kappa itself is a contested statistic for thematic accuracy, because chance agreement is not clearly relevant to map users and kappa adds little to the information in overall and per-class accuracy; the practical recommendation is to report the confusion matrix, per-class user's and producer's accuracy and area-adjusted estimates (Stehman, 1997). The present matrix gives only reference-row percentages, so producer's accuracy is available but user's accuracy is not. Reference samples were also not described in terms of

design (random, stratified, or purposive), and the matrix includes a very large "outside" count of 22,422 pixels that should not influence accuracy.

The practical reading of the accuracy results is that the map is reliable for settlement, water, waste land and fallow land, and acceptable for the broad cultivated class, but that the split between dense and medium agriculture is uncertain. The cause is probably spectral: both are green vegetation on a January date with a continuum of canopy density, and a hard boundary between them is arbitrary. Two remedies are available. One is to merge the two classes into a single "cropland with vegetation" class for area statistics and to retain density as a continuous index such as NDVI. The other is to add training samples from fields verified on the ground for crop type and canopy cover. Deep-learning classifiers have shown clear gains over classic methods where large labelled samples are available (Zhao et al., 2023; Digra et al., 2022), but in a district where only a few training polygons exist the first remedy is more realistic.

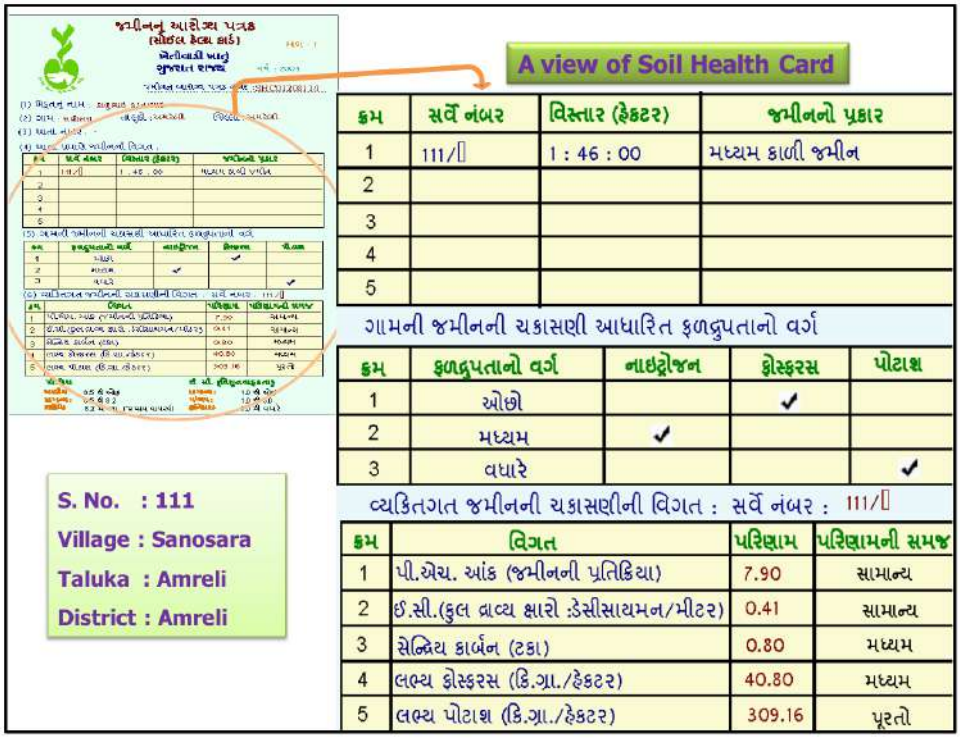
Soil fertility and reaction from Soil Health Cards

Soil Health Cards for the seven villages show a consistent pattern (Table 4). Available nitrogen was medium in six of the seven villages and not in the medium class in Mangvapal. Available phosphorus was low in six villages with the exception of Bhandariya Mota, and available potash was high in every village. Soil reaction was normal (6.5-8.2) and electrical conductivity below 1 dS m^{-1}, indicating no salinity problem at the plots sampled. Organic carbon at the village level was mostly medium to optimum, with only small areas in the low class.

Table 4. Dominant soil health class in the seven selected villages, based on Soil Health Card records

Attribute	Dominant class	Exceptions among the seven villages
Available nitrogen	Medium	Mangvapal (not medium)
Available phosphorus	Low	Bhandariya Mota (not low)
Available potash	High	None
Organic carbon	Medium to optimum	Small low-class area (Sanosara)
pH	Normal (6.5-8.2)	None
Electrical conductivity	Normal (<1 dS m^{-1})	None

The cards themselves are bilingual, with farmer, village, taluka, survey number and nutrient values (Fig. 10). Their regular format is what allows automated joining to cadastral polygons.



ક્રમ	સર્વે નંબર	વિસ્તાર (હેકટર)	જમીનનો પ્રકાર
1	111/	1 : 46 : 00	મધ્યમ કાળી જમીન
2			
3			
4			
5			

ગામની જમીનની ચકાસણી આધારિત ફળદ્રુપતાનો વર્ગ

ક્રમ	ફળદ્રુપતાનો વર્ગ	નાઇટ્રોજન	ફોસ્ફરસ	પોટાશ
1	ઓછો		✓	
2	મધ્યમ	✓		
3	વધારે			✓

વ્યકિતગત જમીનની ચકાસણીની વિગત : સર્વે નંબર : 111/

ક્રમ	વિગત	પરિણામ	પરિણામની સમજ
1	પી.એચ. આંક (જમીનની પ્રતિક્રિયા)	7.90	સામાન્ય
2	ઈ.સી.(કુલ દ્રાવ્ય ક્ષારો :ડેસીસાયમન/મીટર)	0.41	સામાન્ય
3	સેન્દ્રિય કાર્બન (ટકા)	0.80	મધ્યમ
4	લભ્ય ફોસ્ફરસ (કિ.ગ્રા./હેકટર)	40.80	મધ્યમ
5	લભ્ય પોટાશ (કિ.ગ્રા./હેકટર)	309.16	પૂરતો

Fig. 10. Example of a Soil Health Card for a farmer's field in Sanosara village (survey no. 111)

Maps for Sanosara show how these records look when tied to cadastral polygons. Nitrogen was medium and phosphorus low wherever a card was available (Fig. 11). Potash was high on all mapped plots, and organic carbon varied from low through medium to optimum, with optimum plots clustered in the north and east (Fig. 12). pH and electrical conductivity were in the normal class on all mapped plots (Fig. 13).

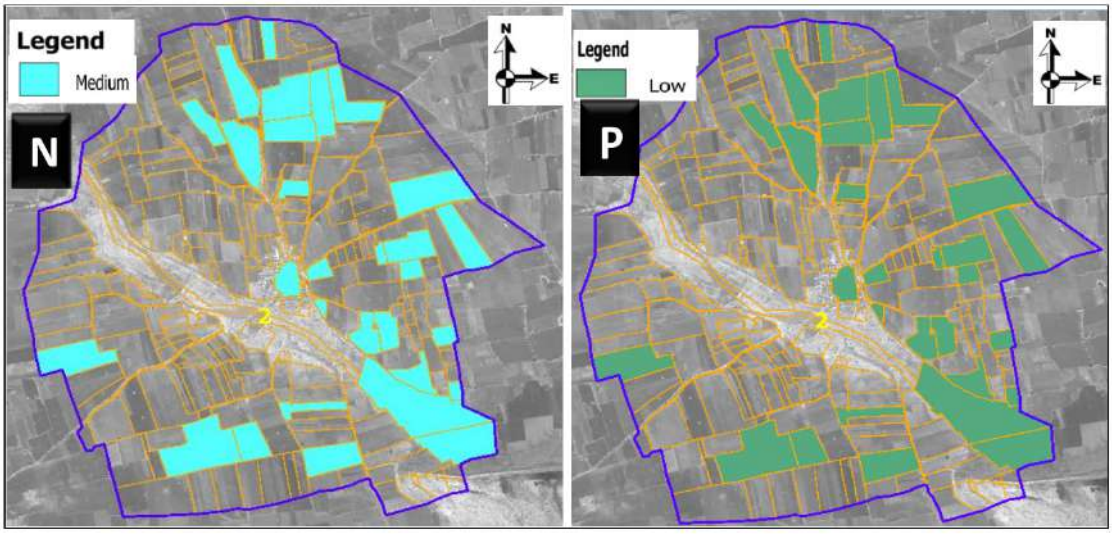


Fig. 11. Nitrogen (left) and phosphorus (right) status of soils in Sanosara village based on Soil Health Cards

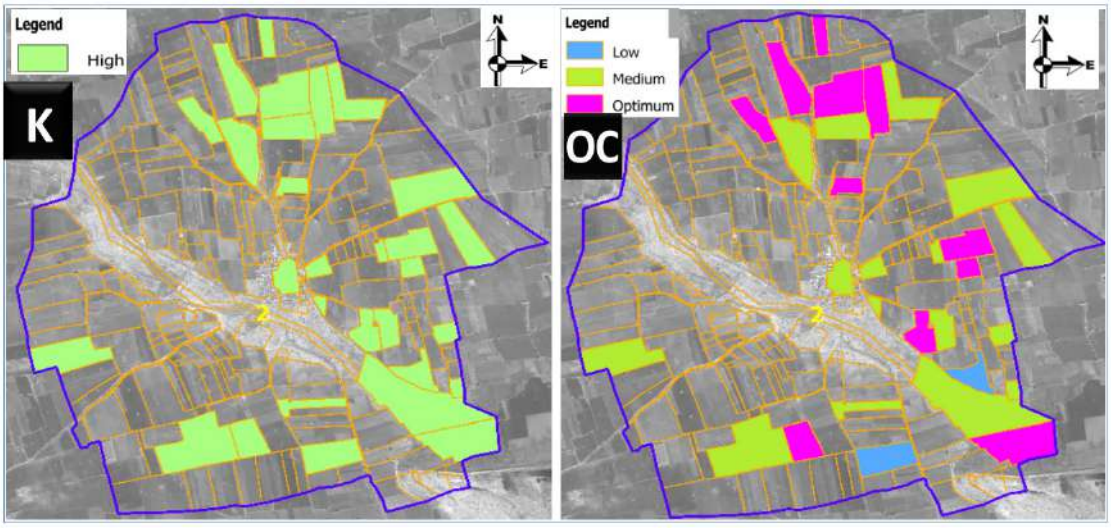


Fig. 12. Potash (left) and organic carbon (right) status of soils in Sanosara village based on Soil Health Cards

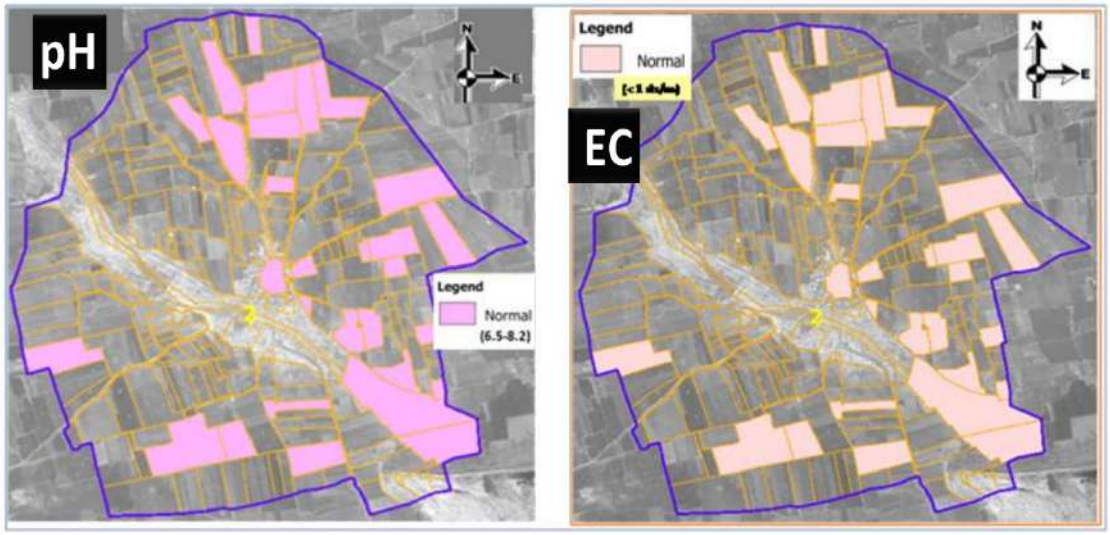


Fig. 13. Cadastral-level pH (left) and electrical conductivity (right) status of Sanosara village

Agronomically, the pattern of medium nitrogen, low phosphorus and high potash implies that fertiliser recommendations should emphasise phosphorus and nitrogen and that potash application can be deferred on most plots. The Soil Health Card scheme was designed for precisely this purpose, and its reported benefits, including yield increases of 5-6% and fertiliser reductions of 8-10% in the reviewed evidence (Timisina et al., 2025), depend on farmers acting on plot-specific advice. Mapping the cards turns a stack of individual documents into a village-level overview that extension staff can use to identify clusters of plots with the same deficiency. In Sanosara, for example, the plots without a mapped card form large contiguous blocks that could be prioritised for sampling. Linking cards to a decision tool in this way follows earlier proposals for balanced fertilisation (Thiyageshwari et al., 2006).

Two features of the maps limit their interpretation. First, only plots with an SHC are coloured, so the maps document where data exist rather than the complete fertility pattern; wherever cards are absent the map is blank. Second, the cards report qualitative classes and not numerical values, so gradients within a class are lost. The review of broad-scale digital soil mapping stresses that models and maps are only as good as the sampling that underlies them and that well-designed sampling schemes are needed (Chen et al., 2022). The cards were collected under an administrative scheme rather than a statistical design, and their spatial coverage is determined by who participated.

The thesis extends the findings from seven villages to the entire taluka by assuming that the pattern holds. That extrapolation is an assumption and is not tested here. Remote sensing covariates, such as terrain attributes, soil colour from imagery and vegetation indices, are used in

digital soil mapping to extend point observations spatially (Richer-de-Forges et al., 2023), and a model of this kind trained on the plot cards, with independent validation on withheld villages, would be the defensible way to produce a taluka-wide fertility surface.

Integration for micro-level planning

The three components of the workflow, parcel-level cadastral overlays, a taluka-wide land cover map and plot-level soil health maps, answer different planning questions. The land cover map shows how much land is under vigorous crop, how much is fallow and where settlements and waste land lie; it is the tool for allocation questions at the taluka or cluster level. The cadastral overlay on high-resolution imagery lets field staff locate any survey number, check field condition and plan visits. The SHC maps support input planning, especially fertiliser recommendations, at village and plot scale. Combined in one geodatabase, the three layers allow queries such as "which survey numbers under dense cropping in January have low phosphorus?" or "which fallow plots have good fertility and could be brought under irrigation?" Such integrated databases follow the logic of earlier GIS-based decision support systems for district and local planning in India (Archarya et al., 2011; Gupta et al., 2001; Bariar et al., 2004) and of watershed-oriented resource mapping (Krishna, 1996; Kerr et al., 2002). Reviews of agricultural remote sensing note that the real value of mapped products lies in their coupling with agronomic and management data and not in the maps alone (Alami Machichi et al., 2023; Joshi et al., 2023; Wu et al., 2023).

Several steps would increase the operational value of the workflow: (i) merging uncertain classes and reporting accuracy with a transparent sample design; (ii) adding a second image date to separate permanent from seasonal fallow and to infer cropping intensity; (iii) automating the extraction of field boundaries from CARTOSAT-1 or LISS-IV, so that cadastral digitisation need not be repeated manually for every village, as work on boundary delineation suggests is feasible (Zheng et al., 2026); and (iv) linking the SHC database through a unique survey-number identifier so that updates after each two-year card cycle flow automatically into the maps.

IV. LIMITATIONS

The study has several limitations that readers should keep in mind. The imagery dates from 2006 to 2009 and the maps describe the land of that period; land use in the taluka, particularly irrigation, has probably changed since. The classification used a per-pixel maximum-likelihood classifier on a 23.5 m image, with no texture or object-based information and no ancillary data, and it has the known tendency of the maximum-likelihood rule to confuse classes with overlapping distributions. The accuracy figures in the source are internally inconsistent, a pixel-weighted recalculation gives lower overall accuracy than the figure reported, the reference sampling design is undocumented, and one dense-agriculture sub-class is poorly separated. Class areas are therefore uncertain by an unknown margin, and no area-adjusted estimates with confidence intervals were produced.

The cadastral work lacks a quantified positional error, and the CARTOSAT-1 scene predates the soil data by several years. The Soil Health Card data are qualitative, restricted to seven villages chosen at random but not stratified by soil or land cover, and mapped for only one village in detail. Organic carbon, nitrogen and phosphorus classes depend on laboratory methods and threshold values that are not given on the cards reproduced here. Joined polygons are limited to plots with a card.

V. CONCLUSION

A workflow combining georeferenced CARTOSAT-1, LISS-IV and LISS-III imagery, digitised cadastral boundaries and Soil Health Card records was applied to Amreli Taluka to provide land cover and soil fertility information at the scale of villages and survey numbers. The LISS-III classification showed that cultivated land with dense, medium or poor vegetation covered 64.73% of the taluka, fallow land 16.81%, habitation 12.01%, waste land 4.73% and water 1.71%. The classification performed well for most classes but separated dense from medium agriculture poorly, and the reported accuracy indices should be treated as an upper bound; overall accuracy was probably between 70 and 80%. Soil Health Card records for seven villages showed medium nitrogen, low phosphorus and high potash, with normal pH and electrical conductivity, a pattern that supports phosphorus-focused fertiliser advice. Mapping the cards at survey-number level for Sanosara demonstrated how farm-scale records can be turned into spatial tools for extension. The approach is transferable and inexpensive, but it should be strengthened by transparent accuracy assessment, multi-date imagery, automated field boundary extraction and a validated spatial model for extending the soil data beyond the sampled plots.

ACKNOWLEDGEMENTS

The satellite data and GIS facilities were provided by the Bhaskaracharya Institute for Space Applications and Geo-informatics (BISAG), Gandhinagar. Meteorological and field information were supplied by Junagadh Agricultural University and the farmers of Amreli Taluka.

REFERENCES

[1] Acharya, P.S., Ghosh, S.K. and De Sarkar, S.C. 2011. Natural resources data management system (NRDMS) a suite of web-accessible geo-spatial data processing tools for e-Governance in India. In *Proceedings of the 2nd International Conference on Computing for Geospatial Research & Applications* (pp. 1-1). https://doi.org/10.1145/1999320.1999380.

[2] Alami Machichi, M., Mansouri, L.E., Imani, Y., Bourja, O., Lahlou, O., Zennayi, Y., Nourzeix, F., Houmma, I.H. and Hadria, R. 2023. Crop mapping using supervised machine learning and deep learning: A systematic literature review. *International Journal of Remote Sensing*, **44**(8): 2717-2753. https://doi.org/10.1080/01431161.2023.2205984.

[3] Bariar, A., Gupta, R.D. and Prasad, S.C. 2004. Development of GIS based spatial data infrastructure for micro-level planning. In *Map World Forum. Hyderabad, India*.

[4] Bastiaanssen, W.G., Molden, D.J. and Makin, I.W. 2000. Remote sensing for irrigated agriculture: examples from research and possible applications. *Agricultural water management*, **46**(2): 137-155. https://doi.org/10.1016/S0378-3774(00)00080-9.

[5] Burrough, P.A. 1989. Matching spatial databases and quantitative models in land resource assessment. *Soil Use and Management*, ***5***(1): 3-8. https://doi.org/10.1111/j.1475-2743.1989.tb00753.x

[6] Chen, S., Arrouays, D., Mulder, V.L., Poggio, L., Minasny, B., Roudier, P., Libohova, Z., Lagacherie, P., Hannam, J., Meersmans, J., Richer-de-Forges, A.C. and Walter, C. 2022. Digital mapping of GlobalSoilMap soil properties at a broad scale: A review. *Geoderma*, **409**: 115567. https://doi.org/10.1016/j.geoderma.2021.115567.

[7] Digra, M., Dhir, R. and Sharma, N. 2022. Land use land cover classification of remote sensing images based on the deep learning approaches: a statistical analysis and review. *Arabian Journal of Geosciences*, **15**(10): 1003. https://doi.org/10.1007/s12517-022-10246-8.

[8] Gupta, R.D., Garg, P.K. and Arora, M. 2001. A GIS Based Decision Support System for Developmental Planning in Dehradun District. *J. Indian Cartogr*, **21**.

[9] Joshi, A., Pradhan, B., Gite, S. and Chakraborty, S. 2023. Remote-sensing data and deep-learning techniques in crop mapping and yield prediction: A systematic review. *Remote Sensing*, **15**(8): 2014. https://doi.org/10.3390/rs15082014.

[10] Kasturirangan, K. 1995. Remote Sensing in India—Present scenario and future thrusts. *Journal of the Indian Society of Remote Sensing*, **23**(1): 1-6. https://doi.org/10.1007/BF02997429.

[11] Kerr, J.M., Pangare, G. and Pangare, V. 2002. *Watershed development projects in India: an evaluation* (Vol. 127). Intl Food Policy Res Inst.

[12] Krishna, A.P. 1996. Remote sensing approach for watershed based resources management in the Sikkim Himalaya: a case study. *Journal of the Indian Society of Remote Sensing*, **24**(2): 71-83. https://doi.org/10.1007/BF03016119.

[13] Largueche, F.Z.B. 2006. Estimating soil contamination with Kriging interpolation method. *American Journal of Applied Sciences*, **3**(6): 1894-1898.

[14] Lillesand, T.M., Kiefer, R.W. and Chipman, J.W. 2015. Remote Sensing and Image Interpretation. John Wiley & Sons, New York.

[15] Macarringue, L.S., Bolfe, É.L. and Pereira, P.R.M. 2022. Developments in land use and land cover classification techniques in remote sensing: A review. *Journal of Geographic Information System*, **14**(1): 1-28. https://doi.org/10.4236/jgis.2022.141001.

[16] Markon, C.J. 2003. A temporal study of urban development for the municipality of Anchorage, Alaska. *GeoCarto International*, **18**(3): 21-33. https://doi.org/10.1080/10106040308542278.

[17] Puri, S.K. 2007. Integrating Scientific with Indigenous Knowledge: Constructing Knowledge Alliances for Land Management in India1. *MIS quarterly*, **31**(2): 355-379. https://doi.org/10.2307/25148795.

[18] Richer-de-Forges, A.C., Chen, Q., Baghdadi, N., Chen, S., Gomez, C., Jacquemoud, S., Martelet, G., Mulder, V.L., Urbina-Salazar, D., Vaudour, E., Weiss, M., Wigneron, J.P. and Arrouays, D. 2023. Remote sensing data for digital soil mapping in French research—a review. *Remote Sensing*, **15**(12): 3070. https://doi.org/10.3390/rs15123070.

[19] Stehman, S.V. 1997. Selecting and interpreting measures of thematic classification accuracy. *Remote sensing of Environment*, **62**(1): 77-89. https://doi.org/10.1016/S0034-4257(97)00083-7.

[20] Thiyageshwari, S., Natesan, R., Boopathi, P.M., Paulraj, C. and Natarajan, S. 2006. Soil health sustenance tools to ensure balanced fertilization-DSSIFER and Soil Health Card.

[21] Timilsina, R.R., Khosla, S., Rahut, D.B., Jena, P.R. and Sonobe, T. 2025. A comprehensive review of the soil health status for enhancing agricultural sustainability. *Frontiers in Environmental Science*, **13**: 1548095. https://doi.org/10.3389/fenvs.2025.1548095.

[22] Wu, B., Zhang, M., Zeng, H., Tian, F., Potgieter, A.B., Qin, X., Yan, N., Chang, S., Zhao, Y., Dong, Q., Boken, V., Plotnikov, D., Guo, H., Wu, F., Zhao, H., Deronde, B., Tits, L. and Loupian, E. 2023. Challenges and opportunities in remote sensing-based crop monitoring: A review. *National Science Review*, **10**(4): nwac290. https://doi.org/10.1093/nsr/nwac290.

[23] Zhao, S., Tu, K., Ye, S., Tang, H., Hu, Y. and Xie, C. 2023. Land use and land cover classification meets deep learning: A review. *Sensors*, *23*(21), 8966. https://doi.org/10.3390/s23218966.

[24] Zheng, J., Ye, Z., Wen, Y., Huang, J., Zhang, Z., Li, Q., Hu, Q., Xu, B., Zhao, L. and Fu, H. 2026. A comprehensive review of agricultural parcel and boundary delineation from remote sensing images: Recent progress and future perspectives. *IEEE Geoscience and Remote Sensing Magazine*. doi: 10.1109/MGRS.2026.3658493.